Carrier-Mediated Magnetoelectric Coupling in Functionalized Graphene

Elton J. G. Santos*

School of Engineering and Applied Sciences, Harvard University, Cambridge, Massachusetts 02138, United States, Department of Chemical Engineering, Stanford University, Stanford, California 94305, United States, and SLAC National Accelerator Laboratory, SUNCAT Center for Interface Science and Catalysis, Menlo Park, California 94025, United States

ABSTRACT Materials in which magnetic order and electric fields can be coupled are of high fundamental and technological interests. Electrical control of magnetism is not only important for ultralow power consumption applications, but also enables control over intrinsic material properties that may have a major step in new developments in spintronic and magnetoelectric devices. Here we show that the magnetism induced by aryl-radicals covalently functionalized on top of multilayer graphene is sensitive to external electric fields which coupled to the interlayer charge-imbalance yields a strong magnetoelectric coupling. We used first-principles simulations, taking into account van der Waals dispersion forces, to show that this effect is thickness-dependent: it increases dramatically to thicker graphene structures reaching magnetoelectric coefficients comparable to perovskite interfaces. The interplay between electric fields and magnetism also leads functionalized graphene layers to a fully polarized spin state (half-metallicity). Efficiency nearly to 100% spin-polarization is observed at low electric bias, and the selection of the spin-conducting channel is determined by the field polarization.

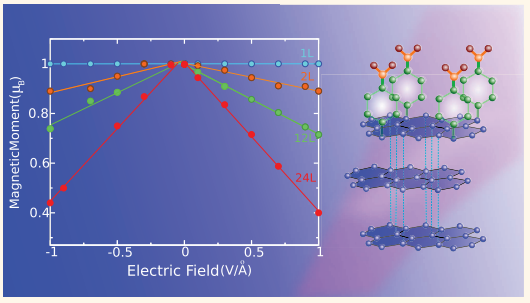

KEYWORDS: magnetoelectric coupling · multilayer graphene · electric field control of magnetism · functionalization · half-metal · carrier

The control of the magnetic polarization **M** through an electric field $\boldsymbol{\varepsilon}$ as well as the electric polarization **P** through a magnetic field **H** has provided a pathway toward next generation of multifunctional electronic devices. Materials that present such magnetoelectric response are usually inorganic materials such as perovskites, transition metals oxides (e.g., CrO_2), or multiferroics composites, where the coupling between charge and spin is substantial.[1,2] A few organic multiferroic compounds are known[3−5] and a search for light-molecular solids that may result in cheap, flexible, and easy to produce magnetoelectric devices has started. In particular, the weak spin−orbit and hyperfine interactions in organic materials are one of the main reasons to attract this interest. This allows maintaining the spin information over large distances and to obtain spin-relaxation times that exceed the time detected in inorganic materials by orders of magnitude.[6,7] Recently, graphene, chemically functionalized by adatoms,[8−11] and nitrophenyl diazonium molecules (NPD)[12−14] has shown a magnetic behavior that could be controlled by electric fields.[12,15] This has open the prospect of new graphene devices where magnetic information can be manipulated *via* electrical means.

Here we present detailed first-principles calculations that show that an external $\boldsymbol{\varepsilon}$ not only control the magnetic properties of functionalized multilayer graphene, but also generate a strong spin-charge coupling that induces a magnetoelectric effect in a purely organic system. The effect is tunable with the number of layers, increasing in magnitude to thicker structures. The magnetoelectric coefficients α, used to characterize the size of the coupling between $\boldsymbol{\varepsilon}$ and **M**, are in the range of $6.49-200.0 \times 10^{-14}$ G cm^2/V. These values are comparable in magnitude to those found in thin films based on 3*d* transition metals (Fe, Co, and Ni), perovskite interfaces, and half-metals. The observed dependence of magnetic properties of functionalized graphene on the external field is due to the spin-dependent carriers driven by the bias at the graphene surface. At low bias, the system also displays a transition to a half-metallic state with spin-polarization close to 100% at the Dirac cones.

* Address correspondence to eltonjos@stanford.edu.

Received for review July 22, 2013 and accepted October 23, 2013.

Published online November 11, 2013
10.1021/nn4037877

This suggest that spin currents can be achieved in graphene materials using well-known surface chemical routes widely applied to engineer and tailor novel properties in carbon materials.

RESULTS

We use NPD molecules as a test-case molecule because their ferromagnetic signal has recently been measured and a preferential functionalization to one of the graphene sublattices was observed.[12−14] Figure 1a, shows the magnetic moment $M = S$ as a function of ε for positive and negative field polarizations. The magnetic moment is calculated as the integral of the magnetization density over the supercell using well-converged parameters at each value of the applied electric field. Only the spin component of total magnetic moment is taken into account due to the small orbital components. At low number of layers, for instance monolayer (1L) and bilayer (2L), graphene shows a negligible $S(\varepsilon)$-dependence, slightly keeping its value of 1.0 μ_B per NPD molecule at zero electric field. As the number of layers increases, substantial modifications of S as a function of the external field is displayed. For multilayer graphene, 12L and 24L, S tunes from its zero-field magnitude (1.0 μ_B) to 0.4 μ_B per molecule roughly following a linear damping with ε. Using the variation of S for each value of ε is possible to show that at 41 graphene layers the value of moment goes to zero at ε = 1.0 V/Å. This indicates that the magnetism generated *via* NPD molecules on multilayer graphene can work as molecular-switch driven by the electric bias between on and off spin-states. This is in good agreement with superconducting quantum interference device (SQUID) experimental results recently obtained for magnetic centers in graphene.[15] We observed that the applied electric bias of the intensity used here can be obtained and controlled as recently reported, using HfO_2 gates. Electric fields as high as 6 V/nm were achieved across of few-layers graphene.[16] We have also performed calculations at different NPD coverages on top of graphene in the range of 3.1 to 0.8%. We observed that the tuning of the magnetic moment at low concentrations is stronger with a faster decay with the applied electric field. At the low-dilution limit studied (0.8%) variations of 100% in the value of the magnetic moment, that is, from 1.0 μ_B per molecule to zero, are obtained for fields close to 0.4 V/Å in bilayer graphene.

In the following, we calculate the quantity that characterizes the coupling of S and ε in functionalized multilayer graphene, that is, the magnetoelectric coefficient α. This is given by

$$\alpha_{ij} = \mu_0 \left(\frac{\partial S_i}{\partial \varepsilon_j} \right) \quad (1)$$

where μ_0 is the vacuum magnetic permeability constant. Only components along the z-direction are

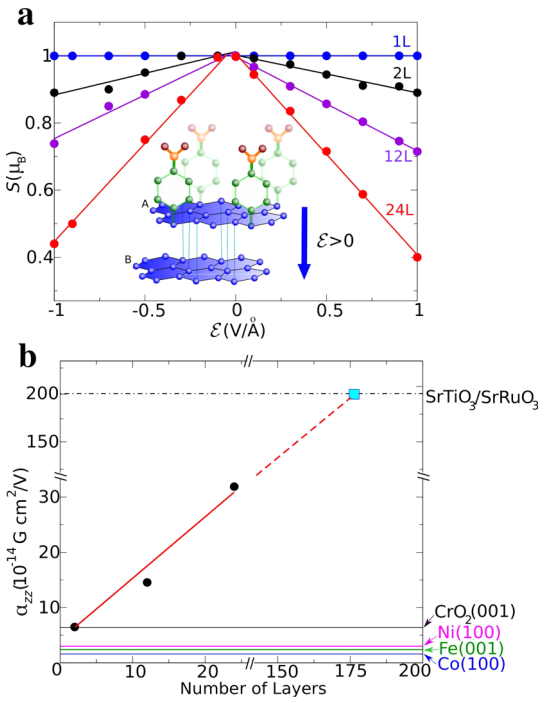

Figure 1. (a) Spin moment $S(\mu_B)$ vs the external field ε(V/Å) for different number of layers: 1L, 2L, 12L, and 24L. The Bernal AB stacking was used in all calculations. The solid curves are linear fits to the calculated data shown by filled symbols. The inset shows a schematic geometry of NPD molecules on top of a bilayer graphene. The blue arrow shows the orientation of $\varepsilon > 0$. The adsorbate coverage is 12.5%. (b) α as a function of the number of graphene layers. The calculated data is shown by the black symbols linearly fitted by the solid line. The extrapolation of the data is shown by the dashed line with the filled square at 176 layers. For comparison, the horizontal lines show the value of α for Co(100) (solid blue), Fe(001) (solid green), Ni(100) (solid pink), CrO_2(001) (solid black), and $SrTiO_3/SrRuO_3$ (dashed black).

evaluated since the major contribution of the spin moment comes from the S_z projection. Performing a data fitting to the results shown in Figure 1a using eq 1 gives α_{zz} in the limits of $6.03-32.2 \times 10^{-14}$ G cm^2/V, as shown in Figure 1b. These values are several times larger than those found in 3*d* transition metal layer films (e.g., Fe(001), Co(0001), Ni(001)),[17] but relatively smaller that those obtained in perovskite interfaces ($SrRuO_3/SrTiO_3$).[18] The extrapolation of our data given in Figure 1b shows that at ~176 layers the magnetoelectric coefficient corresponds to $\alpha_{zz} = 2 \times 10^{-12}$ G cm^2/V. This points that thicker graphene samples could give similar magnetoelectric response as that for perovskite interfaces.

The origin of the dependence of α_{zz} with the number of layers is shown schematically in Figure 2. The application of an external electric field ε generates a polarization charge density $\Delta\rho$ which is mainly localized at the NPD molecule and at the bottom graphene layer. This gives rise to a dipole moment density in the slab that partially screens the electric field over the screening length of the layers. The

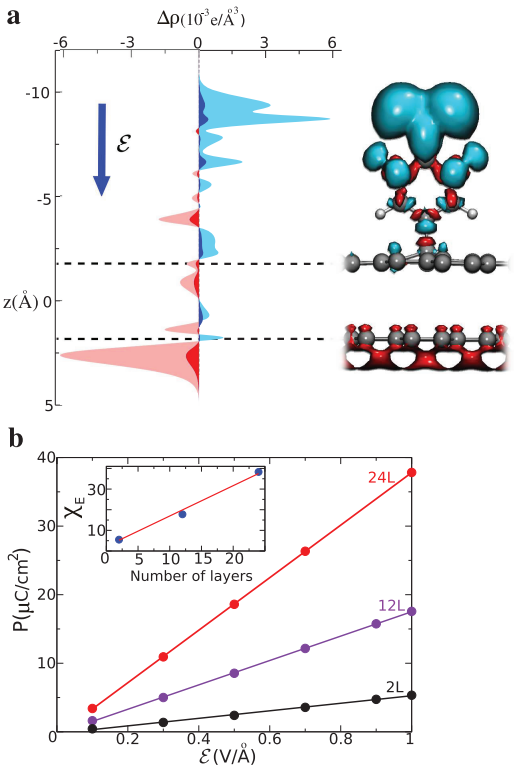

Figure 2. (a) On the left, induced charge densities, $\Delta\rho = \rho(\varepsilon) - \rho(0)$, in e/Å^3, between the two C-planes. The bolder and lighter shaded curves correspond to $\varepsilon = 0.1$ V/Å and $\varepsilon = 1.0$ V/Å, respectively. The large blue arrow shows the direction of ε relative to the bilayer structure. On the right, isosurfaces (at ± 0.04 e^-/bohr^3) corresponding to $\Delta\rho$ of NPD molecules on top of graphene (ε = 1.0 V/Å). Positive and negative values are shown in blue and red surfaces. (b) P(μC/cm^2) as a function of ε (V/Å) for 2L−24L graphene. The AB stacking was used for all calculations. The inset shows the electric susceptibility χ_E vs the number of layers; the solid red curve corresponds to a linear fit.

induced charge densities $\Delta\rho$ at different fields are shown in Figure 2a. The overall polarization charge is field-dependent and increases in magnitude with the external field intensity. The integration of $\Delta\rho$ along the direction perpendicular to the layers (z coordinate), using the equation $\nabla \cdot \mathbf{P}(\mathbf{r}) = -\Delta\rho(\mathbf{r})$ for each field polarization results in a polarization P that is shown in Figure 2b. The dependence of P on $\boldsymbol{\varepsilon}$ follows the equation $P = \varepsilon_0 \chi_E \boldsymbol{\varepsilon}$, where ε_0 is the vacuum permittivity and χ_E is the electric susceptibility. This shows a linear response of the functionalized multilayer graphene on the electric bias which can be related to α_{zz} through $\alpha_{zz} = \mu_0((\partial P)/(\partial \varepsilon))((\partial S_z)/(\partial P))$. As the linear increment in P is compensated by the linear damping of S_z, that is, the derivative $((\partial S_z)/(\partial P)) \sim 1$. This gives $\alpha_{zz} = \mu_0 \varepsilon_0 \chi_E$, which shows that the magnetoelectric coefficient is proportional to the electric susceptibility as plotted in the inset of Figure 2b.

There is an additional effect when an external electric field is applied on a spin-polarized surface which is the driving of carriers at a specific spin-state on the C-plane: half-metallicity. Figure 3a shows the

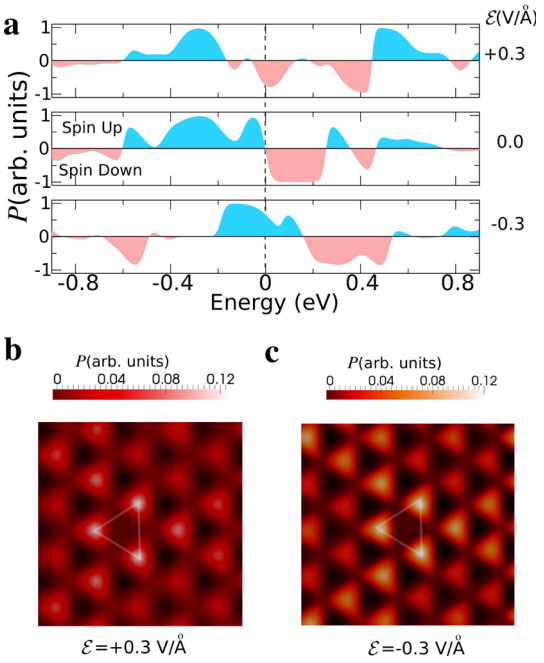

Figure 3. Spin polarized states induced by NPD molecules on top of bilayer 2L graphene. (a) P (arb. units) as a function of the energy (eV) at zero and finite ($\varepsilon = \pm 3.0$ V/Å) electric fields. Polarization for up and down spins are shown for positive (blue curve) and negative (faint red curve) values of P, respectively. The vertical dashed line shows E_F, which is set to zero in each panel. (b, c) show the surface cross section of $\xi(r)$ (at ± 0.02 e^-/bohr^2) at its maximum value at positive ($\varepsilon = +0.3$ V/Å) and negative electric fields ($\varepsilon = -0.3$ V/Å). Note that P is largely originated at the first C-neighbors of the defect site forming the triangle shape-like density.

spin polarization P for a functionalized bilayer graphene versus energy E. P is defined as a function of the spin-dependent density of states $N_\sigma(E)$ ($\sigma = \uparrow$ or $\downarrow$) through the equation $P = (N_\uparrow(E) - N_\downarrow(E))/(N_\uparrow(E) + N_\downarrow(E))$ for an energy interval close to the Fermi level (E_F). At finite fields, $\boldsymbol{\varepsilon} = +0.30$ V/Å, only one spin-conducting channel (spin down) is present around E_F, which results in full spin-polarization ($|P| \rightarrow 100\%$). Once the electric field orientation is reversed, $\boldsymbol{\varepsilon} = -0.30$ V/Å, a similar effect is observed but with the other spin-conducting channel (spin up) instead. Looking at the cross section of the spatial distribution of the spin polarization density $\xi(\mathbf{r})$ given by $\xi(\mathbf{r}) = (\rho_\uparrow(\mathbf{r}) - \rho_\downarrow(\mathbf{r}))/(\rho_\uparrow(\mathbf{r}) + \rho_\downarrow(\mathbf{r}))$, where $\rho_\sigma(\mathbf{r})$ is the volumetric spin density, the main contribution for this spin-polarized effect comes from the first carbon neighbors to the adsorption site, as plotted in Figure 3b,c, for two field polarizations. This is in good agreement with scanning tunneling microscopy and $I-V$ measurements performed for NPD molecules chemisorbed on top of graphene samples with 5−10 layers.[12] At $\boldsymbol{\varepsilon} = 0.0$ V/Å both spin-conducting channels contribute at E_F, and no polarization is observed. Our calculations also show that the energy difference between half-metallic states and that with no polarization is large. For the thickest system studied (24L), the half-metallic state is most stable by 38.4 meV per carbon

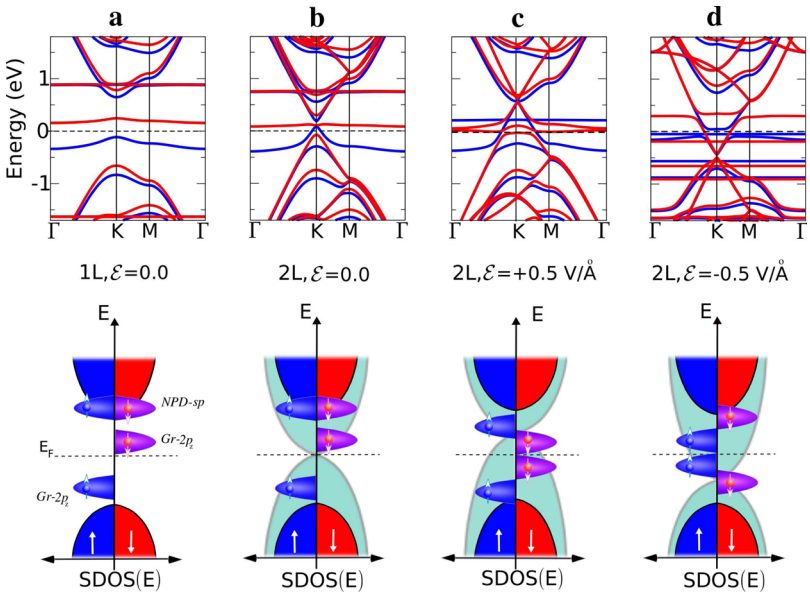

Figure 4. Spin polarized band structures (top panels) and density of states (bottom panels) for functionalized graphene layers. (a, b) Electronic structure for monolayer 1L and bilayer 2L at $\varepsilon = 0$. (c, d) Changes in the electronic structure of the bilayer at finite fields: $\varepsilon = +0.5$ V/Å and -0.5 V/Å, respectively. Blue and red lines show spin up and spin down states, respectively. Defect levels are marked with their respective characters (*sp* and $2p_z$) for NPD molecules and graphene host. E_F is set to zero for each system and is shown by the dashed line.

atom at $\varepsilon = \pm 0.50$ V/Å. This energy is higher than that obtained to the edge states of graphene nanoribbons, which has a polarization energy of ~20 meV per atom.[19] The higher magnetic stabilization energy for functionalized multilayer graphene might open a new route to obtain half-metallic behavior in carbon materials.

In the following we discuss the underlying mechanism of the electric-control of magnetism in functionalized graphene. Figure 4 shows the calculated band structures of monolayer 1L and bilayer 2L graphene with NPD molecules on the top layer at different values of ε. In monolayer 1L graphene (Figure 4a), the adsorbates induce a dispersionless defect-state that appears at E_F. It has a majority $2p_z$ contribution from the three C-atoms nearest to the adsorption site with a magnetic moment of 0.29 μ_B/atom. The adsorbate has small contribution to the defect state with a magnetic moment of less than ~0.01 μ_B. The half-filled character of this $2p_z$-defect band combined with its dispersion-less behavior induces a spin-splitting of ~0.34 eV between up and down states which is observed above room temperature. Two-degenerated states from the NPD molecule are found at 0.85 eV above E_F, which are composed mainly of *sp*-electrons. Some other states localized at the graphene surface also suffer a splitting due to the spin polarization induced by the defect although it is smaller than that for the $2p_z$ states close to E_F. The polarization of the Dirac cone is mainly appreciated by a 0.20 eV energy-splitting at the *K*-point. It is worth noting that these features (dispersionless state at E_F strongly localized in the opposite sublattice to the adsorbate, appearance of a large spectral gap) are consistent with the spectral changes expected around the Dirac point for a number of vacancies distributed on the same sublattice.[20,21] Indeed, for the p_z band of graphene the presence of a covalently bound molecule is largely equivalent to the formation of a vacancy, since electronic hopping is suppressed through the p_z orbital at the binding site. This observed magnetic behavior follows closely the expectation based on Lieb's theorem[22] for a bipartite Hubbard model at half-filling, which is an appropriate approach to understand the low-energy electronic excitations in graphene.

Once the second layer is attached in a 2L graphene, a Dirac cone is created at *K* that couples with the $2p_z$-defect bands at E_F. A modification in the dispersion of both spin up and spin down levels is appreciated, with a shift to higher and lower energies by ~200 and ~139 meV, respectively. At $\varepsilon = 0$, both 1L and 2L graphene are still at the neutrality point and a negligible charge-transfer between the molecule and the C-plane maintains the defect levels at similar position (Figure 4a,b). For finite fields, 1L graphene does not suffer any substantial modifications in its electronic energy levels keeping their original dispersion even at high fields. The bilayer 2L graphene, in its turn, shows a sizable effect that is observed to depend on the field strength. The coupling between the $2p_z$-defect bands of the functionalized layer and the Dirac cone of the second pristine layer is electric-sensitive and can be driven by the bias. The Dirac cone of the pristine layer is shifted up or down relative to the defect states, which generates an interlayer charge-transfer that changes the spin polarization induced by the NPD molecules. These effects are appreciated in Figure 4c,d, which displays the magnetic behavior for positive ($\varepsilon = +0.50$ V/Å) and

negative ($\varepsilon = +0.50$ V/Å) electric fields, respectively. An energy shift by +0.46 eV and −0.53 eV is noted around the Fermi energy which stabilizes a specific set of spin polarized states (down or up) that are bias-dependent. As the amount of spin-polarization is mainly due to a single spin character, the half-metallicity is developed. At higher electric fields, the opposite spin states gradually start to be occupied, inducing the decrease in the magnetic moment. It is worth noting that the shift observed for the Dirac cone agrees very well with that observed using SQUID measurements[15] on sp^3 adsorbates, such as F and H, which was ~0.45 eV. This also indicates that the physics behind of this behavior is independent of the used adsorbate where similar results were obtained in our calculations using NPD molecules. A theoretical foundation for such effect despite the chemical and biological character of the adsorbate has recently been proposed which describes in detail the noted phenomenon.[23] This theory is based on the close relation between the electronic structure of single C−C bond between the adsorbate and the graphene surface and that observed for a π-vacancy in a disorder model for graphene.[20,21] When a single covalent bond is established with the sheet, a local moment of 1.0 μ_B always appear in the system as an effect of the localized states that get pinned at the Fermi level. This breaks the symmetry between the sublattices and induces a behavior that is largely independent of the chemical and biological activity of the adsorbate, as long as a weakly polar bond is present.

CONCLUSIONS

In summary, the interplay between electric fields and magnetism in functionalized multilayer graphene is reported based on first-principles density functional theory simulations. The described interplay helps to explain experimentally observed results and predict a novel set of magnetoelectric properties where light electrons (2*s* and 2*p*) play an important role. This electric-field mediated tuning of the magnetic properties provides an additional degree of freedom in the design and modification of graphene-based materials, opening new possibilities for efficient control of spintronic device properties.

METHODS

The simulations presented are based on density-functional-theory calculations as implemented in the SIESTA code.[24] The generalized gradient approximation,[25] double-ζ plus polarized basis set, norm-conserving Troullier-Martins pseudopotentials[26] were used to simulate the systems. The resolution of the real-space grid used to calculate the Hartree and exchange-correlation contribution to the total energy was chosen to be equivalent to 150 Ry plane-wave cutoff. Calculations using nonlocal van der Waals density functional[27] were also performed, and it gives similar results. Atomic coordinates were allowed to relax using a conjugate-gradient algorithm until all forces were smaller than 0.01 eV/Å. Relevant lattice constants (in-plane and out-of-plane) were optimized for each system taking into account the applied electric field. Calculations performed using a different layer stacking, for example, rombohedral (ABC), shows a similar tuning of the magnetic moment as a function of the electric bias. To avoid interactions between layer images the distance between the graphene monolayers along the direction perpendicular to the C-atom plane was always set larger than 25 Å. A 60 × 60 × 1 *k*-sampling grid in the two-atom unit cell of graphene gives well converged values for all the calculated properties.[28] A sawtooth-like potential perpendicular to the graphene planes is utilized to simulate the external electric field in the supercell. The system is stable up to fields close to 1.5 V/Å, where the layers are observed to be weakly bound. Constrained calculations using fixed-spin moment[29,30] were utilized to calculate the magnetic moment at its energetic minimum for some of the graphene systems subjected to electric fields. This enforce that the observed magnetism is variationally unique and avoid fluctuations on the value of the spin moment with the bias. In addition, localized states at the molecules (NO_2 radical), electrically driven by the field, get pinned at the Fermi level, which resulted in numerical instabilities in the self-consistent loop. A map of the dependence of the total energy on the magnetization was used to fix this problem.

Conflict of Interest: The authors declare no competing financial interest.

Acknowledgment. We thank Efthimios Kaxiras for a critical reading of the manuscript and Sakhrat Khizroev and Robert C. Haddon for valuable discussions regarding their experiments on NPD molecules on multilayer graphene. First principles calculations were performed using computational resources provided under allocation supported by National Science Foundation Grant Nos. TG-DMR120049 and TG-PHY120021 on the Extreme Science and Engineering Discovery Environment (XSEDE).

REFERENCES AND NOTES

1. Fiebig, M. Revival of the Magnetoelectric Effect. *J. Phys. D: Appl. Phys.* **2005**, *38*, 123–153.
2. Vaz, C. A. F.; Hoffman, J.; Ahn, C. H.; Ramesh, R. Magnetoelectric Coupling Effects in Multiferroic Complex Oxide Composite Structures. *Adv. Mater.* **2010**, *22*, 1521–4095.
3. Kagawa, F.; Horiuchi, S.; Tokunaga, M.; Fujioka, J.; Tokura, Y. Ferroelectricity in a One-Dimensional Organic Quantum Magnet. *Nat. Phys.* **2010**, *6*, 169–172.
4. Giovannetti, G.; Kumar, S.; Stroppa, A.; van den Brink, J.; Picozzi, S. Multiferroicity in TTF-CA Organic Molecular Crystals Predicted through *Ab Initio* Calculations. *Phys. Rev. Lett.* **2009**, *103*, 266401–266405.
5. Ren, S.; Wuttig, M. Organic Exciton Multiferroics. *Adv. Mater.* **2012**, *24*, 724–727.
6. Zutic, I.; Fabian, J.; Das Sarma, S. Spintronics: Fundamentals and Applications. *Rev. Mod. Phys.* **2004**, *76*, 323–410.
7. Harris, C. B.; Schlupp, R. L.; Schuch, H. Optically Detected Electron Spin Locking and Rotary Echo Trains in Molecular Excited States. *Phys. Rev. Lett.* **1973**, *30*, 1019–1022.
8. Xie, L.; Wang, X.; Lu, J.; Ni, Z.; Luo, Z.; Mao, M.; Wang, R.; Wangand, Y.; Huang, H.; Qi, D.; *et al.* Room Temperature Ferromagnetism in Partially Hydrogenated Epitaxial Graphene. *Appl. Phys. Lett.* **2011**, *98*, 193113–193116.
9. McCreary, K. M.; Swartz, A. G.; Han, W.; Fabian, J.; Kawakami, R. K. Magnetic Moment Formation in Graphene Detected by Scattering of Pure Spin Currents. *Phys. Rev. Lett.* **2012**, *109*, 186604–186608.
10. Hong, X.; Zou, K.; Wang, B.; Cheng, S.-H.; Zhu, J. Evidence for Spin-Flip Scattering and Local Moments in Dilute Fluorinated Graphene. *Phys. Rev. Lett.* **2012**, *108*, 226602–226607.
11. Nair, R. R.; Sepioni, M.; Tsai, I. L.; Lehtinen, O.; Keinonen, J.; Krasheninnikov, A. V.; Thomson, T.; Geim, A. K.; Grigorieva,

I. V. Spin-Half Paramagnetism in Graphene Induced by Point Defects. *Nat. Phys.* **2012**, *8*, 199–202.
12. Hong, J.; Bekyarova, E.; Liang, P.; de Heer, W. A.; Haddon, R. C.; Khizroev, S. Room-Temperature Magnetic Ordering in Functionalized Graphene. *Sci. Rep.* **2012**, *2*, 624.
13. Hong, J.; Niyogi, S.; Bekyarova, E.; Itkis, M. E.; Ramesh, P.; Amos, N.; Litvinov, D.; Berger, C.; de Heer, W. A.; Khizroev, S.; *et al.* Effect of Nitrophenyl Functionalization on the Magnetic Properties of Epitaxial Graphene. *Small* **2011**, *7*, 1175–1180.
14. Niyogi, S.; Bekyarova, E.; Hong, J.; Khizroev, S.; Berger, C.; de Heer, W.; Haddon, R. C. Covalent Chemistry for Graphene Electronics. *J. Phys. Chem. Lett.* **2011**, *2*, 2487–2498.
15. Nair, R. R.; Tsai, I. L.; Sepioni, M.; Lehtinen, O.; Keinonen, J.; Krasheninnikov, A. V.; Castro Neto, A. H.; Geim, A. K.; Grigorieva, I. V. Dual Origins of Defect Magnetism in Graphene and its Reversible Switching by Molecular Doping. *Nat. Commun.* **2013**, *4*, 2010.
16. Zou, K.; Zhang, Fan; Clapp, C.; MacDonald, A. H.; Zhu, J. Transport Studies of Dual-Gated ABC and ABA Trilayer Graphene: Band Gap Opening and Band Structure Tuning in Very Large Perpendicular Electric Fields. *Nano Lett.* **2013**, *13*, 369–373.
17. Duan, C. G.; Velev, J. P.; Sabirianov, R. F.; Zhu, Z.; Chu, J.; Jaswal, S. S.; Tsymbal, E. Y. Surface Magnetoelectric Effect in Ferromagnetic Metal Films. *Phys. Rev. Lett.* **2008**, *101*, 137201–137205.
18. Rondinelli, J. M.; Stengel, M.; Spaldin, N. A. Carrier-Mediated Magnetoelectricity in Complex Oxide Heterostructures. *Nat. Nanotechnol.* **2008**, *3*, 46–50.
19. Son, Y. W.; Cohen, M. L.; Louie, S. G. Half-Metallic Graphene Nanoribbons. *Nature* **2006**, *444*, 347–349.
20. Pereira, V. M.; Guinea, F.; Lopes dos Santos, J. M. B.; Peres, N. M. R.; Castro Neto, A. H. Disorder Induced Localized States in Graphene. *Phys. Rev. Lett.* **2006**, *96*, 036801–036805.
21. Pereira, V. M.; Lopes dos Santos, J. M. B.; Castro Neto, A. H. Modeling Disorder in Graphene. *Phys. Rev. B* **2007**, *77*, 115109–115126.
22. Lieb, E. H. Two Theorems on the Hubbard Model. *Phys. Rev. Lett.* **1989**, *62*, 1201–1204.
23. Santos, E. J. G.; Ayuela, A.; Sánchez-Portal, D. Universal Magnetic Properties of sp^3-Type Defects in Covalently Functionalized Graphene. *New J. Phys.* **2012**, *14*, 043022–043034.
24. Soler, J. M.; Artacho, E.; Gale, J. D.; Garcia, A.; Junquera, J.; Ordejon, P.; Sánchez-Portal, D. The SIESTA Method for *Ab Initio* Order-N Materials Simulation. *J. Phys.: Condens. Matter* **2002**, *14*, 2745–2779.
25. Perdew, J. P.; Burke, K.; Ernzerhof, M. Generalized Gradient Approximation Made Simple. *Phys. Rev. Lett.* **1996**, *77*, 3865–3869.
26. Troullier, N.; Martins, J. L. Efficient Pseudopotentials for Plane-Wave Calculations. *Phys. Rev. B* **1991**, *43*, 1993–2006.
27. Dion, M.; Rydberg, H.; Schröder, E.; Langreth, D. C.; Lundqvist, B. I. van der Waals Density Functional for General Geometries. *Phys. Rev. Lett.* **2004**, *92*, 246401–246405.
28. Monkhosrt, H. J.; Pack, J. D. Special Points for Brillouin-Zone Integrations. *Phys. Rev. B* **1976**, *13*, 5188–5192.
29. Jarlborg, T.; Freeman, A. J. High-Field Susceptibility and Metamagnetism in Pd. *Phys. Rev. B* **1981**, *23*, 3577–3579.
30. Moruzzi, V. L.; Marcus, P. M.; Kubler, J. Magnetovolume Instabilities and Ferromagnetism *versus* Antiferromagnetism in Bulk FCC Iron and Manganese. *Phys. Rev. B* **1984**, *39*, 6957–6961.